Journal of the Korean Physical Society, Vol. 75, No. 8, October 2019, pp. 561∼568

Effects of the Post-Annealing Treatment on the Properties of Ga-Doped SnO_x Thin Films

Hyo In Bang and Eui-Jung Yun*
Department of ICT Automotive Engineering, Hoseo University, Dangjin 31702, Korea

Byung Seong Bae
Department of Display Engineering, Hoseo University, Asan 31499, Korea

(Received 8 July 2019; revised 7 August 2019; accepted 7 August 2019)

We investigated the effects of the post-annealing treatment (PAT) on the properties of Ga-doped tin-oxide (Ga-SnO_x) thin films grown at room temperature by using a radio-frequency magnetron sputtering technique. On the basis of X-ray photoelectron spectroscopy (XPS), dynamic secondary-ion mass spectrometry, X-ray diffraction (XRD), and Hall Effect measurements, we conclude that n-type SnO_2 is the dominant phase in all samples regardless of PAT at low temperatures (25–200 °C). The Sn^{2+} area decreased to 32.5% with increasing temperature up to 150 °C, with a simultaneous increase in the Sn^{4+} area to 59%. This was attributed to a decrease and an increase in the Ga and the oxygen contents in the samples, respectively, which also caused a decrease in the number of oxygen vacancies in the samples treated at higher temperatures. In contrast, XPS on the samples post-annealed at temperatures higher than 150 °C showed results opposite to those of the samples treated at temperatures lower than 150 °C. This indicates that the Ga ions in Ga-doped SnO_x films act as hole acceptors and that heat treatment is useful for controlling the number of oxygen vacancies, Sn^{2+} ions, and Sn^{4+} ions in Ga-doped SnO_x films. In addition, XRD showed that post-annealing did not affect the amorphous phase in the samples.

PACS numbers: 68.37.Xy, 68.49.Sf, 68.55.ag, 68.55.Ln, 73.61.Jc
Keywords: Process parameters, Ga-doped tin-oxide, Sputtering, Bipolar semiconductor, Heat treatment
DOI: 10.3938/jkps.75.561

I. INTRODUCTION

The giant microelectronics revolution requires the production of complementary metal oxide semiconductor (CMOS) elements with high performance n- and p-type oxide thin-film transistors (TFTs). This is because of their advantages, such as low power dissipation and higher density of logic functions on a chip, over n-channel MOS (NMOS) elements [1–8]. As a result, the realization of high-quality n- and p-type oxide semiconductors is an essential issue for the giant microelectronics revolution.

Recently, tin-oxide (SnO_x) thin films have attracted great attention as the active layer in the implementation of flexible TFTs. This is because SnO_x films are bipolar oxide semiconductors (OSs), in which both n- and p-type doping are probable in the same material. In addition, they are inexpensive, thermally durable under oxidizing conditions, and mechanically stable [1–5,7–19]. However, tin-oxide has several problems. Its high carrier concentration has been reported to make TFTs very easy to turn ON. It can also be crystallized easily, producing non-uniformity in the display [18]. These challenges can be solved by doping with appropriate cations acting as carrier suppressors and crystallization stoppers due to the bipolar characteristic of SnO_x. Some dopants, such as aluminum [17,20], zirconium [21], hafnium [22], and fluorine [23], have been studied to enhance the properties of SnO_x-based TFTs. Nitrogen [24,25], indium [25, 26], antimony [25,26], and gallium [27] have also been reported to be good p-type elements in tin dioxide (SnO_2). On the other hand, Bi-doped SnO_2 films [18,28,29], N-doped SnO [26], and Sb-doped SnO_2 films [30–33] reveal n-type properties. Therefore, the same dopants can have different effects on the properties of SnO_x thin films. Among these dopants, Ga appears to be the most effective p-type dopant for tin-oxide films because of its having an ionic radius (0.62 Å) similar to that of Sn^{4+} (0.69 Å) [27]. In particular, tin-oxide films doped with various dopants were prepared using high-temperature (>200 °C) processes, suggesting that the properties of low-temperature-processed SnO_x films need to be optimized to improve the device properties and stability of flexible SnO_x-based TFTs. Hence, we explored in this

*E-mail: ejyun@hoseo.edu; Tel: +82-41-360-4855; Fax: +82-41-360-4859

study, the effects of post-deposition thermal annealing on the properties of Ga-doped SnO_x films post-annealed at low temperatures ($\leq$200 °C) by using a radio-frequency (RF) magnetron sputtering technique.

II. EXPERIMENTS

SnO_x thin films were grown on 300-nm-thick SiO_2-coated 400-μm-thick Si or corning glass substrates at room temperature (RT; 25 °C) by using RF magnetron sputtering from a 99.999% pure SnO (90 atomic%)-Ga (10 atomic%) mixed target with a 2-inch diameter. Mixtures of 99.999% pure argon (Ar) and oxygen (O_2) gases were used as the reaction gases. The O_2 fraction, defined as $\frac{O_2}{Ar+O_2} \times 100$, was fixed at 4%. The target RF power and the working gas pressure were 50 W and 0.667 Pa, respectively. The substrate was rotated at 13 rpm to deposit uniformly thick SnO_x thin films (≈120 nm). For the examination of the effects of thermal annealing on the properties of the samples, the Ga-doped SnO_x thin films were treated by using a hot plate at different temperatures of 25(RT), 125, 150, 175, and 200 °C for 1 hour in air after deposition.

X-ray photoelectron spectroscopy (XPS) measurements were conducted to analyze the contents (at.%) and the chemical bonding states of Ga, Sn, and O in the Ga-doped SnO_x thin films. Dynamic secondary-ion mass spectrometry (D-SIMS) analyses were also carried out to examine the changes in the depth profiles of Ga, Sn, and O in the samples. The electrical properties of the Ga-doped SnO_x thin films were measured at RT by using a Hall-effect measurements system in the van der Pauw configuration after Ohmic contacts had been formed by sputtering of 100-nm-thick Al, followed by alloying at 150 °C in air for 1 hour. The structures of the films were characterized by using X-ray diffraction (XRD) with a Cu Kα_1 radiation source (λ = 0.15406 nm).

III. RESULTS AND DISCUSSION

Table 1 summarizes the contents (at.%) of Ga, Sn, and O, as obtained from XPS, for the series of Ga-doped SnO_x films treated at different temperatures of RT and 125, 150, 175, and 200 °C for 1 hour in air after sample deposition. As indicated in Table 1, the O concentration was higher than the Sn concentration in all the prepared samples, implying that an O-rich phase, such as SnO_2, was dominant. A Ga content of 7.15 at.% was observed in the samples prepared without heat treatment (prepared at RT), indicating that some Ga had diffused into the SnO_x matrix during sputtering deposition. The diffusion of Ga into the SnO_x films can be explained as follows: The electronegativity difference between Ga^{3+} (1.579) and O (3.758) is larger than that between Sn^{4+} (1.706) and O [34]. The stronger binding of Ga to O than that of Sn to O makes it easier for Ga atoms to diffuse into the SnO_x films during sputtering by forming Ga_2O_3, which causes the in-diffusion of Ga into the SnO_x films. Furthermore, the standard enthalpy of formation of Ga_2O_3 (−1089.1 kJ/mol) [35] is much greater than that of SnO_2 (−577.63 kJ/mol) [36], indicating that the formation of Ga_2O_3 is easier than the formation of SnO_2, which induces the in-diffusion of Ga to the SnO_x films. The Ga content decreased with increasing treatment temperature to 150 °C owing to the out-diffusion of Ga from the samples during heat treatment. This out-diffusion of Ga can be explained as follows: The melting point of Ga is 30 °C [37], which makes it easier for Ga atoms to vaporize from the samples during the low-temperature treatment. The samples treated at 150 °C also have an amorphous structure, in which the many point vacancy defects and the short-range order make the diffusion of Ga atoms out of the SnO_x films during the heating process easier and allow more open space in the samples [38]. The diffusion of Ga in disordered materials is much faster than that in ordered materials because disordered materials contain many open spaces for diffusing atoms to migrate by the random jumping about [38]. This causes a lower Ga concentration in the samples treated at a higher temperature. On the other hand, as listed in Table 1, the Ga density in the sample increased with increasing treatment temperature for temperatures higher than 150 °C. This is related to a decrease in out-diffused Ga due to an increase in the amount of Ga metal reacting with O with increasing temperature. Table 1 also indicates that the O content increases with increasing temperature up to 150 °C owing to the diffusion of O into the samples during heat treatment because of the O concentration gradient (an abundance of O is outside the sample, but relatively little O is in the sample). On the other hand, the O content decreases with increasing temperature for temperatures higher than 150 °C. This is because the rate of out-diffusion of O due to the enhancement of vaporized O at a higher temperature is greater than the rate of in-diffusion of O owing to the O gradient. In general, a higher O content increases the annihilation of oxygen vacancy (V_o) donor defects in the films while a larger Ga concentration increases the

Table 1. Summary of the contents (at.%) of Ga, Sn, and O, as obtained from XPS, for the series of Ga-doped SnO_x films prepared in this study.

Post-annealing temperature (°C)	Ga (at.%)	O (at.%)	Sn (at.%)
25 (RT)	7.15	67.89	24.96
125	6.18	68.40	25.42
150	6.16	68.48	25.36
175	6.60	68.15	25.25
200	6.64	67.77	25.59

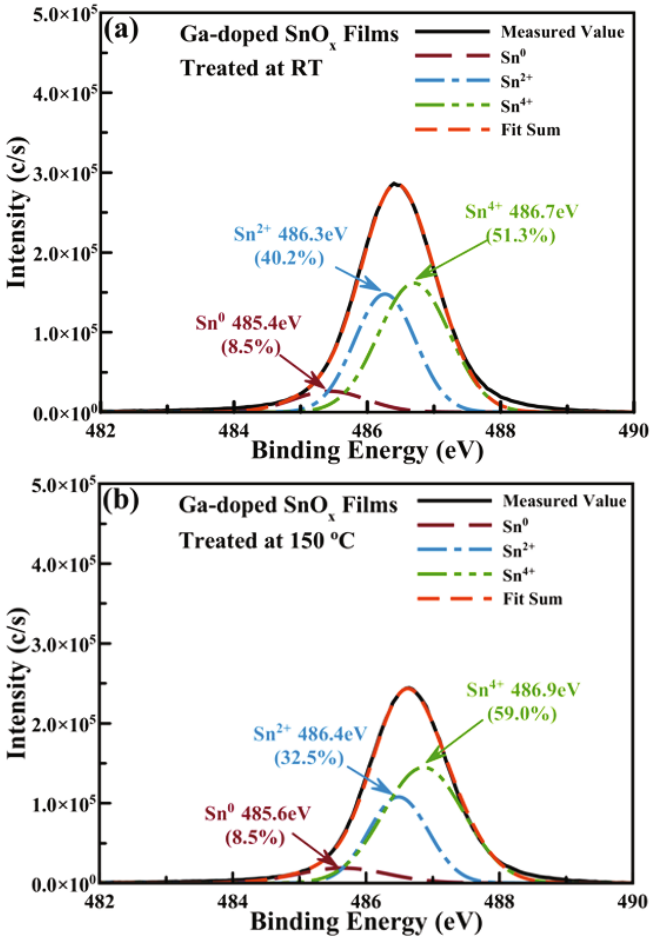

Fig. 1. (Color online) Sn $3d_{5/2}$ XPS spectra were well-fitted using three Gaussian peaks in the Ga-doped SnO_x thin films post-anneal treated at (a) RT (25 °C) and (b) 150 °C.

number of acceptor defects. Therefore, fewer donor and acceptor defects will exist in the samples treated at temperatures from RT to 150 °C whereas more will exist in the samples treated at temperatures greater than 150 °C. We should mention that the contents of Ga, O, and Sn for the series of Ga-doped SnO_x films treated at 300 °C were determined from XPS results to be 6.70, 67.38, and 25.92 at.%, respectively. This result suggests that the properties of the films treated at 200 °C are comparable to those of the films treated at 300 °C.

The carbon (C) 1s reference peak at 284.6 eV was used to calibrate all XPS binding energies. Two Sn 3d XPS peaks, one at 486.3 and the other at 494.7 eV, were observed for all prepared samples, which were related to the Sn $3d_{5/2}$ and the Sn $3d_{3/2}$ spin orbits, respectively [2,6,7,14,15,17,18,39]. Then, the Sn $3d_{5/2}$ XPS spectra of all samples were fitted by using three Gaussian peaks (GPs). Here, three groups of GPs, 485.2–485.6, 486.0–486.4, and 486.5–486.9 eV, were associated with the Sn^0 (metallic Sn), Sn^{2+} (p-type SnO), and Sn^{4+} (n-type SnO_2), respectively.

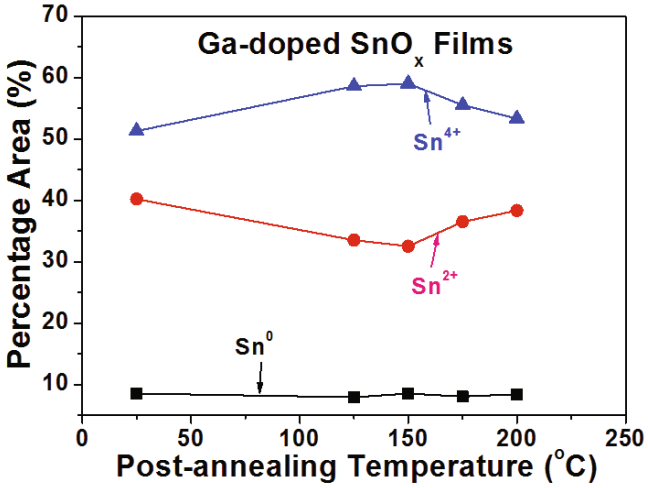

Fig. 2. (Color online) Percentage areas of the three Gaussian peaks (GPs) as functions of the post-annealing temperature for samples post-anneal treated at various temperatures, which were obtained after fitting the Sn $3d_{5/2}$ XPS peaks using the three Sn^0, Sn^{2+}, and Sn^{4+} GPs (see Fig. 1).

Some examples of the Sn $3d_{5/2}$ XPS spectra well-fitted using three GPs for the samples treated at RT and 150 °C are shown in Figs. 1(a) and 1(b), respectively. Figure 1(a) shows that the percentage areas (PAs) of the Sn^0 peaks at 485.4 eV, the Sn^{2+} peaks at 486.3 eV, and the Sn^{4+} peaks at 486.7 eV were 8.5, 40.2, and 51.3%, respectively, for samples treated at RT. In the case of samples treated at 150 °C, the PAs of the Sn^0 peaks at 485.6 eV, the Sn^{2+} peaks at 486.4 eV, and the Sn^{4+} peaks at 486.9 eV were 8.5, 32.5, and 59.0%, respectively, as is evident in Fig. 1(b).

The PAs of the three GPs as functions of the post-annealing temperature for samples treated at various temperatures were obtained after fitting the Sn $3d_{5/2}$ peaks with the Sn^0, Sn^{2+}, and Sn^{4+} GPs (see Fig. 1) and are shown in Fig. 2. The PAs of the Sn^{4+} and the Sn^{2+} peaks were 51.3 and 40.2%, respectively, for the samples treated at RT (Fig. 2), suggesting that the amount of the SnO phase in the sample is smaller than the amount of the SnO_2 phase. This agrees well with the results listed in Table 1. The PAs of the Sn^{4+} and the Sn^{2+} peaks increased and decreased, respectively, with increasing post-annealing temperature up to 150 °C. These were associated with an increase in the number of Sn^{4+} ions caused by the introduction of more O and a decrease in the number of Sn^{2+} ions due to the out-diffusion of Ga acceptors during heat treatment, as shown in Table 1. This result agrees well with the fact that an increase in the amount of O within the SnO_x thin films causes an increase in the concentration of Sn^{4+} ions [40]. Results opposite those for the samples treated at temperatures lower than 150 °C were observed when the post-annealing temperature was increased to more than 150 °C. Figure 2 also suggests that the amount of the n-type SnO_2 phase on

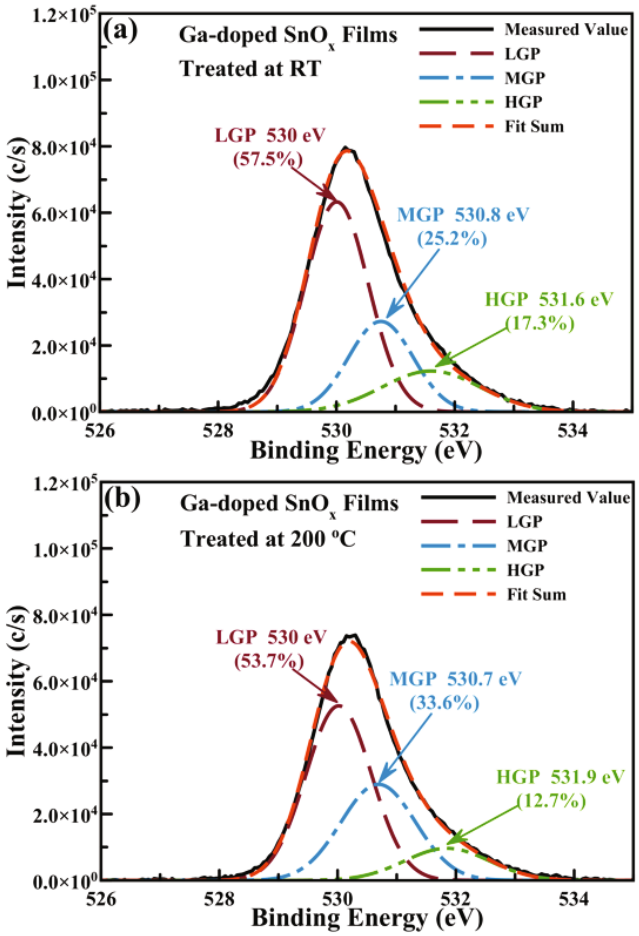

Fig. 3. (Color online) O 1*s* XPS spectra were well-fitted using the low Gaussian peak (LGP), middle Gaussian peak (MGP), and high Gaussian peak (HGP) for Ga-doped SnO_x thin films post-anneal treated at (a) RT (25 °C) and (b) 200 °C.

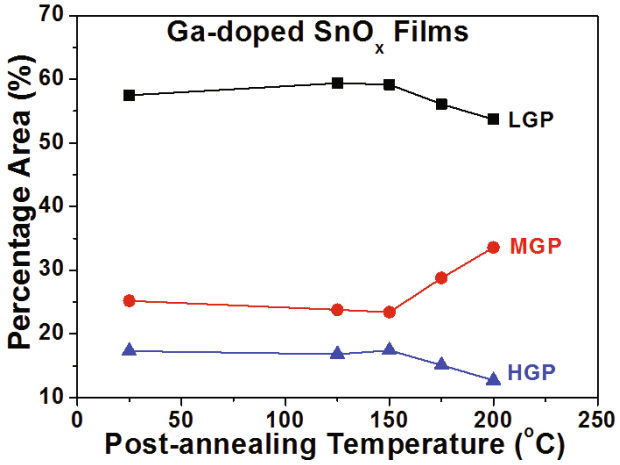

Fig. 4. (Color online) Percentage areas of the three Gaussian peaks as functions of the post-annealing temperature for samples post-anneal treated at various temperatures, which were obtained after fitting the O 1*s* XPS peaks using the low Gaussian peak (LGP), middle Gaussian peak (MGP), and high Gaussian peak (HGP) (see Fig. 3).

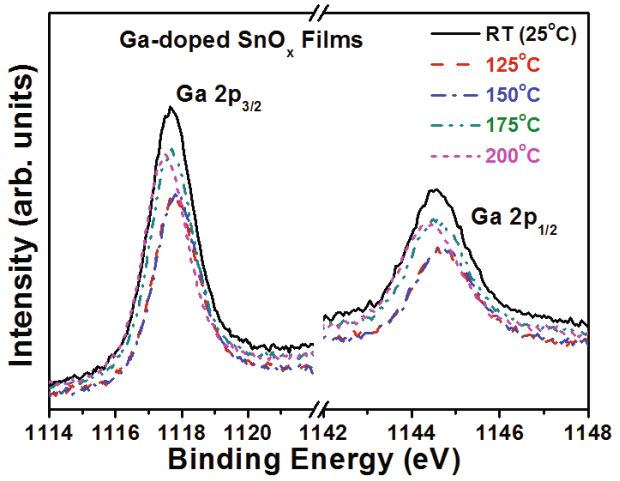

Fig. 5. (Color online) Ga 2*p* XPS spectra for the Ga-doped SnO_x thin films treated at different post-annealing temperatures from RT to 200 °C.

the sample is larger than the amount of *p*-type SnO, regardless of the change in the post-annealing temperature, as is supported by the data in Table 1.

The O 1*s* XPS peaks of all samples were also fitted by using three GPs which are correlated to the low GP (LGP) at around 529.8–530.2 eV, the middle GP (MGP) at 530.4–531.1 eV, and the high GP (HGP) at 531.6–531.9 eV. The LGP was associated with O^{2-} ions in the oxygen-rich regions within the Ga-doped SnO_x matrix whereas the MGP was attributed to O^{2-} ions surrounded by Ga and Sn metal atoms in the oxygen-deficient Ga-doped SnO_x film and was related to V_o defects. The HGP was attributed to chemisorbed or dissociated O or to O-H bonding near the surface of the film [41,42].

Figures 3(a) and 3(b) show some examples of the O 1s XPS peaks fitted using the LGP, MGP, and HGP in the samples treated at post-annealing temperatures of RT and 200 °C, respectively. As plotted in Fig. 3(a), for samples treated at RT, the PAs of the LGP at around 530 eV, the MGP at 530.8 eV, and the HGP at 531.6 eV were 57.5, 25.2, and 17.3%, respectively. On the other hand, Fig. 3(b) shows that the PAs of the LGP at 530 eV, the MGP at 530.7 eV, and the HGP at 531.9 eV were 53.7, 33.6, and 12.7%, respectively, for samples treated at 200 °C.

The PAs of the LGP, MGP, and HGP as functions of the post-annealing temperature for samples treated at various temperatures were obtained after fitting the O 1s peaks with three GPs and are shown in Fig. 4. For samples treated at post-annealing temperatures from RT to 150 °C, the PAs of the LGP and the MGP increased and decreased, respectively, with increasing temperature. The decrease in the MGP area suggests that the in-diffusion of O from the outside the film increased

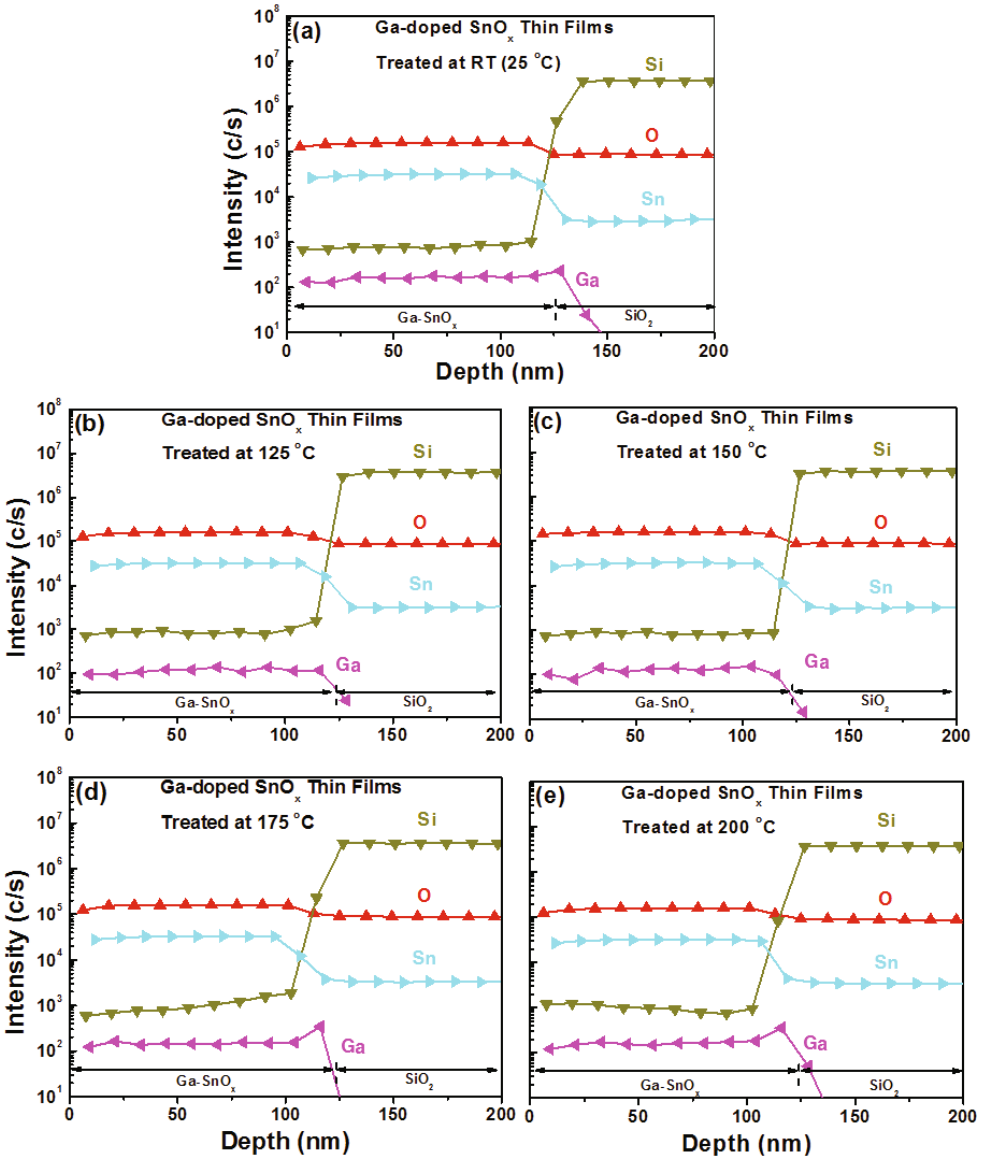

Fig. 6. (Color online) Intensity variations in the tin (Sn), oxygen (O), and gallium (Ga) concentrations with depth in the Ga-doped SnO_x thin films post-annealed at (a) 25(RT), (b) 125, (c) 150, (d) 175, and (e) 200 °C, which were obtained from the D-SIMS depth profiles.

during heat treatment, as confirmed by the data in Table 1, which caused a decrease in the number of V_o's in the films through their annihilation. The increase in the LGP area was also related to the magnification of the reaction of O with Sn metal caused by in-diffused O and out-diffused Ga with increasing temperature, as evidenced by the data in Table 1. However, for the samples treated at post-annealing temperatures higher than 150 °C, a decrease in the LGP area and an increase in the MGP area were observed with increasing temperature. The decrease in the LGP indicated a decrease in the amount of Sn metal reacting with O due to out-diffused O and a decrease in out-diffused Ga with increasing temperature. The increase in the MGP was also attributed to an increase in the number of V_o's, resulting from the increase in out-diffusion of O from the film, as confirmed by the data in Table 1. Figure 4 shows that the HGP area decreased from 17.4 to 12.7% with increasing temperature from 150 to 200 °C. This indicates that the amount of O or H located near the surfaces of the Ga-doped SnO_x thin films decreased with increasing temperature from 150 to 200 °C, which was due to a decrease in the number of defects on the film's surface caused by an increase in in-diffused Ga.

Figure 5 shows the results of XPS analyses for Ga 2p obtained from Ga-doped SnO_x thin films treated at different post-annealing temperatures. For the films treated at RT, two Ga peaks, a Ga $2p_{3/2}$ core level at 1117.7 eV

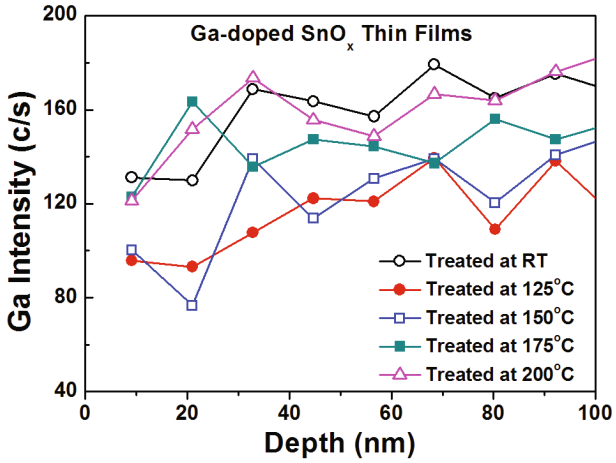

Fig. 7. (Color online) Intensity variations in Ga concentrations with depth in the samples post-annealed at various temperatures, which were obtained from the D-SIMS depth profiles shown in Fig. 6.

and a Ga $2p_{1/2}$ core level at 1144.57 eV (split difference = 26.87 eV.), were observed and can be attributed to pure Ga_2O_3 [27, 43]. Moreover, as the Ga content was decreased due to an increase in post-annealing temperature from RT to 150 °C (see Table 1), the intensities and positions of the two Ga $2p$ peaks, respectively, decreased and shifted to a higher binding energy. With increasing Ga content, however, their intensities and positions increased and shifted to lower binding energy, respectively, due to an increase in the post-annealing temperature from 150 to 200 °C, as shown in Table 1. The observed position changes with Ga content are in good agreement with those reported elsewhere [43]. Hence, the Ga ions in the Ga-doped SnO_x films are in the Ga^{3+} chemical state and act as acceptors in the films, which indicate the substitution of Ga for Sn in the host SnO_2 lattice.

The D-SIMS depth profiles shown in Fig. 6 exhibit the variations in the Ga, Sn, and O concentrations in the Ga-doped SnO_x films for post-annealing treatments at different temperatures. As shown in Fig. 6, the tin concentration was lower than the oxygen concentration in all the prepared samples, confirming the XPS result (Table 1) in that a tin-poor phase, such as SnO_2, was dominant. The Ga content in the samples decreased with increasing temperature up to 150 °C whereas further increases in temperature resulted in an increase in Ga content, which confirmed the result shown in Table 1 and Fig. 5. However, observing the change in the Ga content with temperature with a tendency shown in Fig. 6 was difficult. Therefore, the intensity variations with Ga concentration in the samples post-annealed at various temperatures were obtained from Fig. 6 and are shown in Fig. 7. The changes in the Ga content with increasing temperature shown in Fig. 7 are in good agreement with the data listed in Table 1.

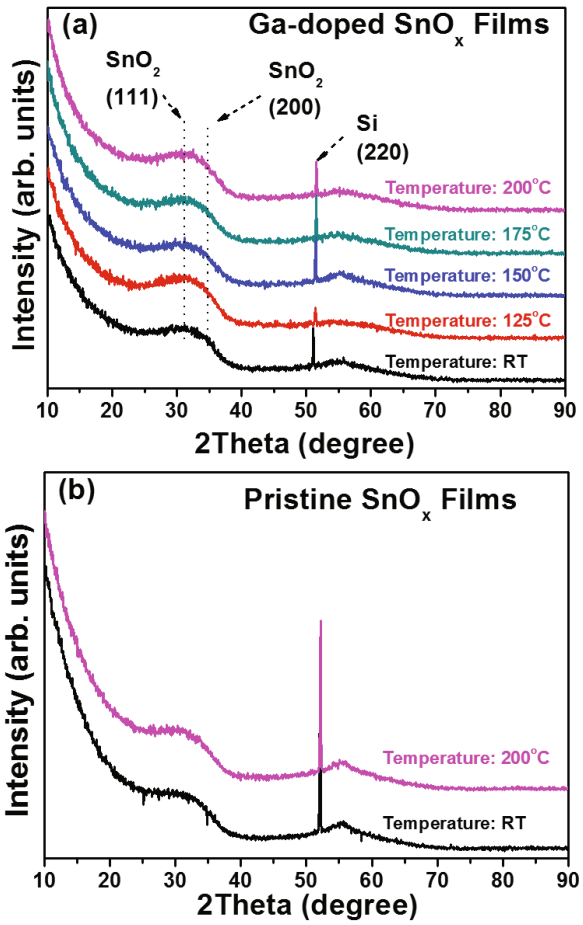

Fig. 8. (Color online) XRD patterns of (a) Ga-doped SnO_x films and (b) pristine SnO_x films undoped with Ga, which were post-annealed at various temperatures from RT (25 °C) to 200 °C.

Figure 8(a) shows the XRD patterns of Ga-doped SnO_x films post-annealed at different temperatures from RT (25 °C) to 200 °C. In general, a large number of defects in the samples can be produced by the fact that the adatom mobility and reactions among Sn, Ga, and O are impeded on the unheated substrate surface during deposition, resulting in the creation of ultrathin nanocrystalline or amorphous films. All samples treated at different annealing temperatures revealed a broad halo peak at around 31.2° 2θ, which was related to a SnO_2 (111) phase (Fig. 8(a)) [2, 6–8, 17]. This indicates that the main n-type SnO_2 phase existed in all samples regardless of post-anneal treatment at low temperatures from RT to 200 °C, which confirmed the XPS result (shown in Table 1 and Fig. 2) and the D-SIMS result (shown in Fig. 6). The XRD patterns of pristine SnO_x thin films undoped with Ga are also shown in Fig. 8(b) to compare their XRD patterns with those of Ga-doped SnO_x films shown in Fig. 8(a). As shown in Fig. 8, the XRD patterns of the Ga-doped SnO_x films were similar to those of the pristine SnO_x thin films.

Table 2. Summary of the Hall effect measurement results at RT for the series of samples post-annealed at different temperatures.

Sample description	Resistivity (Ω·cm)	Hall mobility [$cm^2/(V{\cdot}s)$]	Electron carrier concentration ($1/cm^3$)
Ga-doped SnO_x thin films post-annealed at RT (25 °C)	20.52	5.72	5.49×10^{16}
Ga-doped SnO_x thin films post-annealed at 125 °C	40.56	7.36	2.34×10^{16}
Ga-doped SnO_x thin films post-annealed at 150 °C	94.32	3.95	1.92×10^{16}
Ga-doped SnO_x thin films post-annealed at 175 °C	33.12	4.81	4.27×10^{16}
Ga-doped SnO_x thin films post-annealed at 200 °C	16.08	7.17	5.78×10^{16}

The electrical properties for the series of Ga-doped SnO_x films post-annealed at temperatures from RT to 200 °C were obtained from Hall-effect measurements and are summarized in Table 2. Table 2 shows that the resistivity (ρ), the electron concentration (n), and the mobility (μ) follow the relation $\rho = \frac{1}{nq\mu}$ well, where q is the charge of an electron. Table 2 also shows that n-type conductivity was observed in all samples, regardless of the post-annealing treatment, which supports the XPS, D-SIMS, and XRD results, as shown in Figs. 2, 6, and 8, respectively. As listed in Table 2, with increasing post-annealing temperature from RT to 150 °C, the electron carrier concentration decreased while the resistivity increased. This was attributed mainly to a decrease in the number of oxygen vacancies caused by the introduction of a larger amount of O into the Ga-doped SnO_x thin films, as shown in Table 1 and Fig. 4. That the diffusion of O into the Ga-doped SnO_x films produces in-band gap defects and causes an increase in resistance is worthy of note [18,29]. On the other hand, increasing the post-annealing temperature to more than 150 °C produced results opposite those for the samples treated at temperatures lower than 150 °C, as shown in Fig. 2 and Table 1.

IV. CONCLUSION

In this study, we explored the effects of post-deposition thermal annealing on the properties of Ga-doped SnO_x thin films deposited using a RF magnetron sputtering technique and annealed at low temperatures ($\leq$200 °C). The XPS, D-SIMS, XRD, and Hall effect measurement results suggest that an oxygen-rich n-type SnO_2 is the dominant phase in all samples, regardless of the post-anneal treatment at low temperatures. Furthermore, XRD showed that post-anneal treatment did not affect the amorphous phase in the samples. In the samples post-annealed at temperatures from RT to 150 °C, with increasing temperature, the increase in O and the decrease in Ga in the samples resulted in an increase in the concentration of Sn^{4+} ions and a concomitant decrease in the concentration of Sn^{2+} ions, a decrease in the MGP area and an increase in the LGP area, which in turn caused a decrease in the number of donor and acceptor defects, respectively. In contrast, in the samples post-annealed at temperatures greater than 150 °C, opposite results were obtained in that the concentrations of donor and acceptor defects increased due to a decrease in O and an increase in Ga.

ACKNOWLEDGMENTS

This study was supported by the Academic Research Fund of Hoseo University in 2018 (20180341).

REFERENCES

[1] E. Fortunato, P. Barquinha and R. Martins, Adv. Mater. **24**, 2945 (2012).
[2] L. Guo *et al.*, Mater. Sci. Semicond. Process. **46**, 35 (2016).
[3] L. Qiang *et al.*, Solid-State Electron. **129**, 163 (2017).
[4] J-H. Lee *et al.*, IEEE Electron Dev. Lett. **37**, 300 (2016).
[5] A. Azmi *et al.*, IEEE Electron Dev. Lett. **38**, 1543 (2017).
[6] P-C. Chen *et al.*, J. Alloys Compd. **707**, 162 (2017).
[7] H. Luo, L. Liang and H. Cao, Solid-State Electron. **129**, 88 (2017).
[8] J. S. Ahn, R. Pode and K. B. Lee, Thin Solid Films **608**, 102 (2016).
[9] Y. Ogo *et al.*, Appl. Phys. Lett. **93**, 032113 (2008).
[10] L. Y. Liang *et al.*, J. Electrochem. Soc. **157**, H598 (2010).
[11] J. Um, B. M. Roh, S. Kim and S. E. Kim, Mater. Sci. Semicond. Process. **16**, 1679 (2013).
[12] P. C. Hsu *et al.*, Jpn. J. Appl. Phys. **52**, 05DC07 (2013).

[13] P. C. Hsu *et al.*, Thin Solid Films **555**, 57 (2014).
[14] S-S. Lin, Y-S. Tsai and K-R. Bai, Appl. Surf. Sci. **380**, 203 (2016).
[15] S-S. Lin, S-Y. Fan and Y-S. Tsai, Ceram. Int. **43**, 1802 (2017).
[16] H-J. Kim *et al.*, IEEE Electron Dev. Lett. **38**, 473 (2017).
[17] A. H-T. Nguyen *et al.*, Thin Solid Films **641**, 24 (2017).
[18] J. Yang *et al.*, IEEE Trans. Electron Devices **63**, 1904 (2016).
[19] B. L. Zhu *et al.*, J. Alloys Compd. **719**, 429 (2017).
[20] M. S. Huh *et al.*, Electrochem. Solid-State Lett. **12**, H385 (2009).
[21] X. Zhang *et al.*, Superlattices Microstruct. **123**, 330 (2018).
[22] W-S. Kim *et al.*, Thin Solid Films **520**, 2220 (2012).
[23] B. L. Zhu *et al.*, Ceram. Int. **43**, 10288 (2017).
[24] S. S. Pan *et al.*, Appl. Phys. Lett. **95**, 222112 (2009).
[25] Y. Kim *et al.*, Mater. Sci. Eng. B **177**, 1470 (2012).
[26] Y. Kim, J. Um, S. Kim and S. E. Kim, ECS Solid State Letters **1**, P29 (2012).
[27] H. P. Dang, Q. H. Luc, V. H. Le and T. Le, J. Alloys Compd. **687**, 1012 (2016).
[28] C. Z. Chen *et al.*, Results Phys. **7**, 2588 (2017).
[29] H. I. Bang, H. B. Seo, B. S. Bae and E-J. Yun, Phys. Status Solidi A **216**, 1800863 (2019).
[30] A. Ammari, M. Trari, B. Bellal and N. Zebbar, J. Electroanal. Chem. **823**, 638 (2018).
[31] E. Elangovan and K. Ramamurthi, Cryst. Res. Technol. **38**, 779 (2003).
[32] A. Ammari, M. Trari and N. Zebbar, Mater. Sci. Semicond. Proc. **89**, 97 (2019).
[33] C. Luan, Z. Zhu, W. Mi and J. Ma, J. Alloys Compd. **586**, 426 (2014).
[34] K. Li and D. Xue, J. Phys. Chem. A **110**, 11332 (2006).
[35] W. M. Haynes, *CRC Handbook of Chemistry and Physics* (CRC Press, Boca Raton, 2011).
[36] D. R. Lide, *CRC Handbook of Chemistry and Physics* (CRC Press, Boca Raton, 2009).
[37] V. Y. Prokhorenko *et al.*, High Temp. **38**, 954 (2000).
[38] P. Heitjans and J. Kärger, *Diffusion in Condensed Matter: Methods, Materials, Models* (Springer, Birkhauser, 2005).
[39] D. M. Priyadarshini, R. Mannam, M. S. R. Rao and N. DasGupta, Appl. Surf. Sci. **418**, 414 (2017).
[40] H. Luo *et al.*, ACS Appl. Mater. Interf. **7**, 17023 (2015).
[41] C-H. Hung *et al.*, Mater. Sci. Semicond. Process. **67**, 84 (2017).
[42] H. Xie *et al.*, Mater. Sci. Semicond. Process. **64**, 1 (2017).
[43] H. P. Dang, Q. H. Luc, T. T. Nguyen and T. Le, J. Alloys Compd. **776**, 276 (2019).